



Title	Deep level transient spectroscopic study of oxygen implanted melt grown ZnO single crystal
Author(s)	Ye, ZR; Lu, XH; Ding, GW; Fung, S; Ling, CC; Brauer, G; Anwand, W
Citation	Semiconductor Science And Technology, 2011, v. 26 n. 9, article no. 095016
Issued Date	2011
URL	http://hdl.handle.net/10722/139657
Rights	Semiconductor Science and Technology. Copyright © Institute of Physics Publishing.

Deep level transient spectroscopic study of oxygen implanted melt grown ZnO single crystal

Z. R. Ye, X. H. Lu, G. W. Ding, S. Fung and C. C. Ling

Department of Physics, The University of Hong Kong, Pokfulam Road, Hong Kong, P. R. China

G. Brauer and W. Anwand

Institut für Strahlenphysik, Helmholtz-Zentrum Dresden-Rossendorf, Postfach 510119, D-01314 Dresden, Germany

ABSTRACT

Deep level traps in melt grown ZnO single crystal created by oxygen implantation and subsequent annealing in air were studied by deep level transient spectroscopy measurement between 80K and 300 K. The $E_C-0.29\text{eV}$ trap (E3) was the dominant peak in the as-grown sample and no new defects were created in the as-O-implanted sample. The single peak feature of the DLTS spectra did not change with the annealing temperature up to 750°C , but the activation energy decreased to 0.22 eV. This was explained in terms of a thermally induced defect having a peak close to but inseparable from the original 0.29 eV peak. A systematic study on a wide range of the rate window for the DLTS measurement successfully separated the Arrhenius plot data originated from different traps. It was inferred that the E3 concentration in the samples did not change after the O-implantation. The traps at $E_C-0.11\text{eV}$, $E_C-0.16\text{eV}$ and $E_C-0.58\text{eV}$ were created after the annealing. The $E_C-0.16\text{eV}$ trap was assigned to an intrinsic defect. No DLTS signal was found after the sample was annealed to 1200°C .

I. Introduction

ZnO is a semiconductor having a wide direct band gap ($\sim 3.3\text{eV}$ at room temperature) which has recently attracted a great deal of attention because of its applications in short wavelength optoelectronic devices, spintronic devices, high power and high temperature devices, transparent electronic and further applications [1-4].

Reliable techniques for carrying out n and p-type doping are essential for fabricating semiconductor devices. Despite the asymmetric difficulty in the conductivity doping of ZnO, p-type ZnO was obtained through Group-V element doping (N, As, P and Sb) and Group III-V element co-doping [5].

Ion implantation is a technology frequently used in material and device processing. Selective area doping is one of the advantages of the ion-implantation technology. There have been reports on p-type ZnO layer fabrication achieved by ion implantation [6-16]. However, some workers reported highly resistive n-type material after ion-implantation and subsequent annealing (for example, [12-15]). The ion implantation process would inevitably create undesirable defects and some of these defects would persist even upon a high temperature annealing process. These would include deep traps which would compensate the material.

Other than introducing electrical doping into the ZnO material, 'magnetic doping' of ZnO could also be achieved by transition metal implantation. Room temperature ferromagnetism was reported in ZnO after ion implantation of Co, Ni, C and Fe [16-21], though the mechanism was not yet well understood. Hong et al [22] and

Liu et al [23] have pointed out the influence of intrinsic defects on the magnetic property of transition metal doped ZnO.

All these aspects indicate the importance of a thorough understanding of defects in ZnO for the development of the corresponding ion-implantation technology. However, the defects in ZnO are still not well understood and many controversies remain.

In the present study, deep level transient spectroscopy (DLTS) was used to study the deep traps induced in the melt grown ZnO single crystal induced by O-implantation. Thermal evolution of the deep traps upon annealing in air was also studied. The rate window $(\Delta t)^{-1}$ dependence for the DLTS spectra was studied systemically over a wide range from $\Delta t=0.086-430$ ms.

II. EXPERIMENTAL

The ZnO starting material was a single side polished melt grown n-type, nominally undoped ZnO single crystal ($10 \times 10 \times 0.5$ mm³) obtained from Cermet Inc. with an electron concentration of 8×10^{16} cm⁻³ and an electron mobility of 217 cm² V⁻¹ s⁻¹.

The samples from this material were implanted by oxygen ions on the polished side. The energy of implantation was 150 keV and the fluence was 10^{14} cm⁻². The samples were kept at temperature of 300°C during the implantation. TRIM [24] calculation showed that this resulted in an O-implantation profile with the peak at ~280 nm.

The isochronal annealing step was carried out in a tube furnace in air for a period of 30 minutes. After the annealing, contacts for DLTS measurement were fabricated. The large area Ohmic contact was fabricated by evaporating a 50nm Al film onto the non-polished side of the sample. The Schottky contact was fabricated onto the ion-implanted side of the sample by evaporating Au contacts with a thickness of 50nm after pre-treatment by hydrogen peroxide (details are given in references [25,26]).

DLTS measurements were carried out on these samples across the Schottky and the Ohmic contacts. The contact quality was verified by the I-V and C-V measurements carried out on each of the diodes using the HP4145A semiconductor parameter analyzer and the HP4275A multi-frequency LCR meter, respectively. The DLTS measurements were performed using the Sula DLTS system with temperature varying from 80K to 300K.

The electron emission rate e_n from the trap is given by:

$$e_n = \sigma_n v_{th} N_C \exp[-(E_C - E_a)/kT] \quad (1)$$

where σ_n and E_a are the capture cross section and the activation energy of the deep trap, respectively. N_C and v_{th} are the state density of the conduction band and the velocity of free electron, respectively. As $v_{th} \sim T^{1/2}$ and $\sigma_n \sim T^{3/2}$ holds, the values of E_a and σ_n were obtained from the linear fitting of the Arrhenius plot $\ln(e_n/T^2)$ as a function of T^{-1} [27]. The concentration of the trap N was related to the $\Delta C/C_0$ by:

$$N_T = 2N_d \frac{\Delta C}{C_0} \quad (2)$$

where N_d is the donor concentration, ΔC is the capacitance transient produced with the

rate window $(\Delta t)^{-1}$ and the applied reverse bias of V_R during the emission period, and C_0 is the equilibrium junction capacitance with the reverse bias of V_R .

III. RESULTS AND DISCUSSIONS

DLTS spectra from unimplanted samples were obtained as control. For the as-grown sample, the DLTS spectra had a dominant peak having the activation energy, capture cross section and trap density of $E_a=0.31$ eV, $\sigma_n \sim 10^{-16}$ cm², and $N_T \sim 10^{15}$ cm⁻³, respectively. This trap has parameters agreeing with the commonly found deep trap E3 in ZnO materials [10,15,28-35]. Another peak with $E_a=0.10$ eV, $\sigma_n \sim 10^{-17}$ cm², and $N_T \sim 10^{13}$ cm⁻³ was also identified with a much weaker intensity (20 times less than E3). This trap has the activation energy and the capture cross section close to the previously observed E2 trap [28,30-32]. The E3 intensity dropped with annealing temperature, but persisted at 1200 °C annealing. The $E_a=0.10$ eV level anneals out at 900 °C.

I-V and C-V measurements were carried out on every sample annealed at different temperatures in order to check the quality of the rectifying contacts. The carrier concentrations for each of the samples were also calculated and are tabulated in Table I. The carrier concentration did not undergo a significant change ($n \sim 10^{17}$ cm⁻³) after the O-implantation, and post-implantation annealing up to 900°C. However, the 1200°C post-implantation annealing increased the carrier concentration to $\sim 10^{18}$ cm⁻³.

DLTS spectra of the O-implanted samples were obtained between 80K and 300K

in as-O-implanted state, and after different post-implantation annealing (350°C, 650°C, 750°C, 1200°C). The reverse bias, filling pulse voltage and period were fixed at $V_R=-1$ V, $V_p=0$ V, and $t_p=1$ ms, respectively, for all the DLTS measurements, while the rate window $(\Delta t)^{-1}$ varied over a wide range from $\Delta t =0.086$ ms to 430ms. The application of $V_R=-1$ V to the sample with $n=10^{17}$ cm⁻³ (i.e. the O-implanted samples with annealing temperature $\leq 900^\circ\text{C}$) implied a depletion width of ~ 120 nm, which was within the oxygen implanted region as determined by the TRIM simulation and the SIMS measurement. For the sample annealed at 1200°C, the corresponding depletion width dropped to 38 nm as the carrier concentration increased to $\sim 10^{18}$ cm⁻³.

For the samples annealed at temperatures $\leq 750^\circ\text{C}$, the corresponding DLTS spectra contained a single major carrier peak, implying that the corresponding deep trap was an electron trap. One such typical spectrum series with different Δt 's is illustrated by the spectra obtained from the sample annealed at 750°C and is shown in Figure 1(a). The peaking temperatures and the heights of the DLTS peaks increased with decreasing Δt . The DLTS spectra of the 900°C annealed sample taken with different Δt 's are shown in Figure 1(b), from which three peaks, namely labeled as Peak 1, 2 and 3, were observed. Peak 1 had a much weaker intensity than the other two. For the 1200°C annealed sample, no peak was observed in all the DLTS spectra taken with different rate windows.

The corresponding Arrhenius plots of the DLTS spectra obtained from the as-O-implanted, 750°C and 900°C annealed samples are shown in Figure 2(a). The activation energy E_a of each trap from the different samples was obtained by carrying

out the linear fitting to the Arrhenius plots according to equation (1). The results are shown in Figure 3.

From Figure 3, a single trap with $E_a \sim 0.29\text{eV}$ was identified in the as-O-implanted sample. It was found that its E_a decreases with increasing annealing temperature and drops to a value of 0.22eV at 750°C annealing temperature. After further increase of the annealing temperature to 900°C , three peaks with E_a 's of 0.11eV , 0.16eV and 0.37eV , respectively, were observed.

It is also noticed that the Arrhenius plot data of the 750°C and the peak 3 of the 900°C data significantly deviate from the straight lines obtained from the linear fitting process. However for the as-O-implanted sample, the fitting straight line fitted excellently well with the experimental data. This was clearly illustrated in figure 2(b), which showed the Arrhenius plots of the relevant peaks in a larger scale.

It is worth investigating the drop of the activation energy for the 0.29eV trap, as identified in the as-O-implanted sample, when the annealing temperature increases. One possible explanation was that a new trap having a peaking temperature close to that of the 0.29eV trap was formed by thermal annealing, and the resultant observed peak is the unresolved combination of the two signals.

The DLTS measurement was performed by monitoring the DLTS signal (i.e. the $\Delta C/C$ signal) at different temperatures while temporarily fixing the rate window. For a fixed rate window, each of the traps would have its carrier emission dominant at different temperature, and thus is revealed by a peak in the DLTS spectrum. The peaking temperature is dependent on the trap's emission rate e_n , activation energy E_a ,

capture cross section σ_n , and the rate window adopted. The Arrhenius plot data for a trap can thus be obtained by monitoring the peaking temperatures with the rate window being varied. Two traps (with different E_a 's) having their peaking temperatures too close to be separated would have their emissions dominant at different temperatures. For example for the Arrhenius plots of the 750°C annealed samples (figure 2(b)), the data at the lower temperature region (i.e. $1000/T > 5.2$) corresponded to the emission dominantly contributed from the trap with the lower E_a , and those at the higher temperature region ($1000/T < 5.2$) represented those from the trap having a higher E_a .

In figure 2(b), the as-O-implanted sample data were well fitted by a straight line with $E_a = 0.29\text{eV}$. For the data of the 750°C annealed sample, the data could only be well fitted by two straight lines with the breaking point at $1000/T \sim 5.2$ and the corresponding E_a 's were 0.16 eV and 0.29 eV. Similar two segment line fitting was also carried out on the Arrhenius data of peak 3 for the 900°C annealed sample with the breaking point at $1000/T \sim 5.8$, which yielded the E_a values of 0.30eV and 0.58eV respectively. The two fitted lines also well described the data (figure 2(b)).

The present observation thus suggests that only one trap with $E_a=0.29\text{eV}$ exists in the as-O-implanted and the 350°C annealed samples. However, if the annealing temperature is increased to 750°C, the observed 0.22eV peak was indeed the combined signal from the 0.29eV and the 0.16eV trap, respectively. And if the sample was annealed at 900°C, two unambiguously separated peaks 1 and 2 having an E_a of 0.11eV and 0.16 eV, respectively, were identified. In addition, the observed

0.37eV peak consisted of the 0.30eV trap and the 0.58eV trap, respectively. These findings of the DLTS study in O-implanted ZnO samples are summarized in Table I as well.

A similar DLTS study was also performed on the Schottky contact formed on an n-type N-implanted ZnO sample. The nitrogen implantation process involved a 4-folded implantation with energies of 80, 180, 310 and 500 keV, which produced a 1 μ m-depth box-shaped region with a nitrogen concentration of $\sim 6 \times 10^{18}$ cm $^{-3}$. A similar trap with $E_a = 0.31$ eV was also identified in the as-nitrogen-implanted sample. The annealing behavior of its E_a is included in Figure 3 for comparison to demonstrate that a similar drop of E_a from 0.31eV to 0.25eV in the 750 $^{\circ}$ C annealed sample was also observed after N-implantation. Moreover it was worthy to point out that as compared to the TRIM simulated O-implanted depth profile peaking at ~ 280 nm, the 120nm depletion width corresponding to the reverse bias $V_R = -1$ V during the emission period only barely overlapped the O-ion implantation. It was thus plausible to suggest that the induced defects were formed primarily by the kinetic of vacancy and knock-on in this depletion rather than with the involvement of the implanted oxygen.

The ~ 0.29 eV trap ($\sigma \sim 10^{-16}$ cm 2) found in the as-grown sample and the O-implanted samples had E_a and σ_n in good agreement with those values of the previously reported deep trap E3 [28,30,32]. E3 is the deep trap commonly found in ZnO materials irrespective of the growth method. In the present study, E3 was the major deep trap found in the as-received melt grown sample having $N_T \sim 10^{15}$ cm $^{-3}$. Its density remained unchanged with the O-implantation and the subsequent thermal

annealing up to 900°C. The E3 deep trap has been suggested to be associated with the oxygen vacancy [28] and the zinc interstitial Zn_i [30,32] though no concrete agreement has been reached.

The 0.16eV trap ($\sigma \sim 10^{-17}-10^{-18} \text{ cm}^2$) was observed in the 750°C and the 900°C post-O-implantation annealed samples. Its concentration was $\sim 10^{16} \text{ cm}^{-3}$ in both the 750°C and 900°C annealed samples. A trap having similar E_a ($=0.17-0.18 \text{ eV}$) and σ ($\sim 10^{-16} \text{ cm}^2$) was also identified in the annealed nitrogen implanted (150keV, 10^{14} cm^{-2}) melt grown ZnO samples of our previous study [26], in which the ion-implantation process, annealing process and raw material used were similar to the present study. These two traps are probably the same, i.e. connected to the same lattice defect. We have also carried out DLTS study on electron irradiated (1.8MeV, 10^{15} cm^{-2}) melt grown ZnO samples with the similar raw material and annealing condition. For the 200°C, 350°C and 750°C annealed electron irradiated samples, the DLTS spectra contained two well-separated peaks representing traps having $E_a=0.16-0.18 \text{ eV}$ ($\sigma \sim 10^{-17} \text{ cm}^2$) and $E_a=0.28-0.30 \text{ eV}$ ($\sigma \sim 10^{-16} \text{ cm}^2$). It can be concluded that the 0.16eV trap was created in O-implanted melted grown ZnO single crystal after annealing in air at 750°C, as well as in the electron irradiated samples. As its thermally induced generation was independent of the species of irradiation, this trap should be an intrinsic defect.

In the present study, the 0.58eV ($\sigma \sim 10^{-17} \text{ cm}^2$) trap was identified in the 900°C annealed sample with a concentration of $\sim 10^{16} \text{ cm}^{-3}$. Its activation energy is close to that of the E4 trap having $E_a=0.57 \text{ eV}$ and $\sigma \sim 10^{-12} \text{ cm}^2$ [28]. E4 has been assigned to

the oxygen vacancy [30]. However, the 0.58eV found in the present study had a capture cross section of $\sigma \sim 10^{-17} \text{cm}^2$ only, which is much smaller than the generally accepted value of $\sim 10^{-12} \text{cm}^2$ of E4.

In hydrothermally grown ZnO, Vine et al [33] have identified a 0.58eV trap having a $\sigma \sim 10^{-16} \text{cm}^2$. In a nitrogen implanted and thermally annealed pulsed laser deposition grown ZnO sample, Schmidt et al [35] observed a 0.58eV trap having a $\sigma \sim 10^{-15} \text{cm}^2$ (TN1). It was further argued in ref. [35] that because of the much smaller capture cross section this trap was distinguished from the E4 trap, and is related to nitrogen. The 0.58eV trap, as identified in the present study, is more likely identical with the defect described by Vine et al [33] and Schmidt et al [35] rather than the trap E4, if based on the consideration of the capture cross section.

A 0.11 eV ($\sigma \sim 10^{-18} \text{cm}^2$) trap having a concentration of $\sim 10^{15} \text{cm}^{-3}$ was well separated from the 900°C annealed sample spectra (Peak 1 in figure 1(b)). Its activation energy and capture cross section are close to those values of the E2 trap ($E_a = 0.10 \text{eV}$, $\sigma \sim 10^{-17} \text{cm}^2$) identified in the as-grown sample, and was thus assigned to E2. Our observation thus showed that the 900°C annealing would enhance the E2 concentration from 10^{13}cm^{-3} , as found in the as-grown sample, to 10^{15}cm^{-3} .

No trap was identified in the 1200°C annealed sample irrespective of the rate window. This could imply that all the traps were annealed out (i.e. with concentration below $\sim 10^{14} \text{cm}^{-3}$) at this temperature. However, it should be noted that the reduction of the DLTS signals could be a result of the increased carrier concentration induced by the 1200°C annealing. When fixing the reverse bias during

the DLTS measurements at $V_R=-1V$, the corresponding depletion region width dropped from ~ 120 nm for the $900^\circ C$ annealed sample to ~ 38 nm for the $1200^\circ C$, whereas the carrier concentration increased from $\sim 10^{17} \text{cm}^{-3}$ to $\sim 10^{18} \text{cm}^{-3}$. As the O-implantation profile had a maximum at ~ 280 nm, a shrinking of the depletion region to the Au/ZnO-interface adjacent tail of the implantation profile could result in a reduction of the corresponding DLTS signal.

It is worthy to discuss the limitation of the present study, for which the multi-component peaks were not unambiguously resolved in the DLTS spectra. We have indeed attempted to resolve these peaks by varying the measuring parameters of the DLTS and carrying out Gaussian fitting to the multi-component peak. However we failed to produce a peak separated DLTS spectrum, nor obtain a Gaussian fitting with sufficient statistical certainty. Particular attention would be placed in discussing the Peak 3 found in the $900^\circ C$ annealed sample spectrum. If the peak was fitted with the single component model according to equation (1), it has the $E_a=0.37\text{eV}$ and the capture cross section $\sigma=2\times 10^{13} \text{cm}^2$. From our argument, its Arrhenius plot was fitted separately in two temperature regions and it was concluded to compose of two traps having E_a 's of 0.30eV and 0.58eV . It is noticed that the fitted E_a of 0.37eV coincided with the trap E3' reported previously in ZnO materials [36]. However, the E3' has a capture cross section of $\sigma=7\times 10^{15} \text{cm}^2$ which differs significantly from that of Peak 3 and thus Peak 3 was not originated from the trap E3'.

IV. CONCLUSION

A DLTS study was carried out on O-implanted melt grown ZnO single crystal samples. The $E_C-0.30\text{eV}$ (E3) was the major trap identified in the as-grown sample. The O-implantation process did not create any new deep trap. However, the post-implantation annealing process in air created traps at $E_C-0.16\text{eV}$ and $E_C-0.58\text{ eV}$, respectively, and enhanced the concentration of the E2 trap. The 0.16eV trap is an intrinsic defect.

ACKNOWLEDGEMENTS

This work was supported by the GRF (7031/08P) awarded by the Research Grant Council, HKSAR; the Small Project Grant and the University Development Fund awarded by The University of Hong Kong.

REFERENCES:

- [1] Zinc Oxide Bulk, Thin Films and Nanostructures Processing, Properties and Applications, edited by C. Jagadish and Ss. J. Pearton (Elsevier, New York, 2006).
- [2] Ü. Özgür, Ya. I. Alivov, C. Liu, A. Teke, M. A. Reshchikov, S. Doğan, V. Avrutin, S.-J. Cho and H. Morkoç, *J. Appl. Phys.* **98**, 041301 (2005).
- [3] S. J. Pearton, D. P. Norton, K. Ip, Y. W. Heo and T. Steiner, *J. Vac. Sci. Technol. B* **22**, 932 (2004).
- [4] D. C. Look, *J. Electron. Mater.* **35**, 1299 (2006).
- [5] V. Avrutin, D. J. Silversmith and H. Morkoç, *Proc. IEEE* **98**, 1269 (2010).
- [6] A. N. Georgobiani, A. N. Gruzintsev, V. T. Volkov, M. O. Vorobiev, V. I. Demin and V. A. Dravin, *Nucl. Inst. Meth. Phys. Res. A* **514**, 117 (2003).
- [7] C. C. Lin, S. Y. Chen, S. Y. Cheng, and H. Y. Lee, *Appl. Phys. Lett.* **84**, 5040 (2004).
- [8] H. von Wenckstern, R. Pickenhain, H. Schmidt, M. Brandt, G. Biehne, M. Lorenz, M. Grundmann and G. Brauer, *Appl. Phys. Lett.* **89**, 092122 (2006).
- [9] H. T. Wang, B. S. Kang, J. J. Chen, T. Anderson, S. Jang, F. Ren, H. S. Kim, Y. J. Li, D. P. Norton and S. J. Pearton, *Appl. Phys. Lett.* **88**, 102107 (2006).
- [10] Q. L. Gu, C. C. Ling, G. Brauer, W. Anwand, W. Skorupa, Y. F. Hsu, A. B. Djurišić, C. Y. Zhu, S. Fung and L. W. Lu, *Appl. Phys. Lett.* **92**, 222109 (2008).
- [11] G. Braunstein, A. Muraviev, H. Saxena, N. Dhere, V. Richter and R. Kalish, *Appl. Phys. Lett.* **87**, 192103 (2005).
- [12] X. D. Chen, C. C. Ling, S. Fung, C. D. Beling, Y. F. Mei, R. K. Y. Fu, G. G.

- Siu and P. K. Chu, Appl. Phys. Lett. **88**, 132104 (2006).
- [13] V. Vaithianathan, S. Hishita, J. Y. Park, S. S. Kim, J. Appl. Phys. **102**, 086107 (2007).
- [14] X. D. Zhang, C. L. Liu, Z. Wang, Y. Y. Lu and L. J. Yin, Nucl. Inst. Meth. Phys. Res. B **254**, 83 (2007).
- [15] C. Y. Zhu, C. C. Ling, G. Brauer, W. Anwand and W. Skorupa, Microelectron. J. **40**, 286 (2009).
- [16] K. Potzger, S. Q. Zhou, H. Reuther, A. Mücklich, F. Eichhorn, N. Schell, W. Skorupa, M. Helm, J. Fassbender, T. Hermannsdörfer, T. P. Papageorgiou, Appl. Phys. Lett. **88**, 052508 (2006).
- [17] M. Shuai, L. Liao, H. B. Lu, L. Zhang, J. C. Li, D. J. Fu, J. Phys. D **41**, 135010 (2008).
- [18] S.Q. Zhou, Q Y. Xu, K. Potzger, G. Talut, R. Grötzschel, J. Fassbender, M. Vinnichenko, J. Grenzer, M. Helm, H. Hochmuth, M. Lorenz, M. Grundmann, H. Schmidt, Appl. Phys. Lett. **93**, 232507 (2008).
- [19] K. Potzger, S. Q. Zhou, Q. Y. Xu, A. Shalimov, R. Groetzschel, H. Schmidt, A. Mücklich, M. Helm, J. Fassbender, Appl. Phys. Lett. **93**, 232504 (2008).
- [20] B. Pandey, S. Ghosh, P. Srivastava, P. Kumar, D. Kanjilal, J. Appl. Phys. **105**, 033909 (2009).
- [21] N. Akdogan, H. Zabel, A. Nefedov, K. Westerholt, H. W. Becker, S. Gok, R. Khaibullin and L. Tagirov, J. Appl. Phys. **105**, 043907 (2009).
- [22] N. H. Hong, J. Sakai, N T. Nuong, N. Poirot and A. Ruyter, Phys. Rev. B **72**,

045336 (2005).

[23] H. Liu, X. Zhang, L. Li, Y. X. Wang, K. H. Gao, Z. Q. Li, R. K. Zheng, S. P. Ringer, B. Zhang and X. X. Zhang, *Appl. Phys. Lett.* **91**, 072511 (2007).

[24] J. F. Ziegler, J. P. Biersack, and U. Littmark, *The stopping and range of ions in solids*, (Pergamon, New York, 1985).

[25] Q. L. Gu, C. C. Ling, X. D. Chen, C. K. Cheung, A. M. C. Ng, C. D. Beling, S. Fung, A. B. Djurišić, L. W. Lu, G. Brauer and H. C. Ong, *Appl. Phys. Lett.* **90**, 122101 (2007).

[26] Q. L. Gu, C. K. Cheung, C. C. Ling, A. M. C. Ng, A. B. Djurišić, L. W. Lu, X. D. Chen, S. Fung, C. D. Beling and H. C. Ong, *J. Appl. Phys.* **103**, 093706 (2008).

[27] D. V. Lang, *J. Appl. Phys.* **45**, 3023 (1974).

[28] F. D. Auret, S. A. Goodman, M. J. Legodi, W. E. Meyer, D. C. Look, *Appl. Phys. Lett.* **80**, 1340 (2002).

[29] F. D. Auret S. A. Goodman, M. Hayes, M. J. Legodi, H. A. van Laarhoven, D. C. Look, *Appl. Phys. Lett.* **79**, 3074 (2001).

[30] T. Frank, G. Pensl, R. Tena-Zaera, J. Zúñiga-Pérez, C. Martínez-Tomás, V. Muñoz-Sanjosé, T. Ohshima, H. Itoh, D. Hoffmann, D. Pfisterer, J. Sann, B. Meyer, *Appl. Phys. A* **88**, 141 (2007).

[31] F. C. Auret J. M. Nel, M. Hayes, L. Wu, W. Wesch, E. Wendler, *Superlattices and Microstructures* **39**, 17 (2006).

[32] H. Frenzel, H. v. Wenckstern, A. Weber, H. Schmidt, G. Biehne, H. Hochmuth M. Lorenz and M. Grundmann, *Phys. Rev. B* **76**, 035214 (2007).

- [33] L. Vines, E. V. Monakhov, B. G. Svensson, *Physica B* **404**, 4386 (2009).
- [34] M. Schmidt, M. Ellguth, C. Czekalla, H. von Wenckstern, R. Pickenhain, M. Grundmann, G. Brauer, W. Skorupa, M. Helm, Q. Gu and C. C. Ling, *J. Vac. Sci. Technol. B* **27**, 1597 (2009).
- [35] M. Schmidt, M. Ellguth, F. Schmidt, T. Lüth, H. V. Wenckstern, R. Pickenhain, M. Grundmann, G. Brauer, W. Skorupa, *Phys. Stat. Sol. B* **247**, 1220 (2010).
- [36] F. D. Auret, W. E. Meyer, P. J. Janse van Rensburg, M. Hayes, J. M. Nel, H. von Wenckstern, H. Schmidt, G. Biehne, H. Hochmuth, M. Lorentz and M. Grundmann, *Physica B* **401-402** 378 (2007).

TABLE 1 Tabulated carrier concentration n of the O-implanted samples annealed at different temperatures as obtained by the C-V method. The estimated energy level with respect to the conduction band E_C , the capture cross section σ and the concentration N_T of the deep level traps identified are given also.

<u>Oxygen-implanted ZnO samples</u>				
As-O-implanted $n=2 \times 10^{17} \text{ cm}^{-3}$	350°C $n=3 \times 10^{17} \text{ cm}^{-3}$	750°C $n=1 \times 10^{17} \text{ cm}^{-3}$	900°C $n=4 \times 10^{17} \text{ cm}^{-3}$	1200°C $n=1 \times 10^{18} \text{ cm}^{-3}$
$E_C-0.29\text{eV}$ ($\sigma \sim 10^{-16} \text{ cm}^2$, $N_T = 10^{15} \text{ cm}^{-3}$)	$E_C-0.29\text{eV}$ ($\sigma \sim 10^{-16} \text{ cm}^2$, $N_T = 10^{15} \text{ cm}^{-3}$)	$E_C-0.29\text{eV}$ ($\sigma \sim 10^{-15} \text{ cm}^2$, $N_T \sim 10^{15} \text{ cm}^{-3}$);	$E_C-0.30\text{eV}$ ($\sigma \sim 10^{-15} \text{ cm}^2$, $N_T \sim 10^{15} \text{ cm}^{-3}$);	No peak
		$E_C-0.16\text{eV}$ ($\sigma \sim 10^{-18} \text{ cm}^2$, $N_T \sim 10^{16} \text{ cm}^{-3}$)	$E_C-0.16\text{eV}$ ($\sigma \sim 10^{-17} \text{ cm}^2$, $N_T \sim 10^{16} \text{ cm}^{-3}$);	
			$E_C-0.11\text{eV}$ ($\sigma \sim 10^{-18} \text{ cm}^2$, $N_T \sim 10^{15} \text{ cm}^{-3}$);	
			$E_C-0.58\text{eV}$ ($\sigma \sim 10^{-17} \text{ cm}^2$, $N_T \sim 10^{16} \text{ cm}^{-3}$)	

FIGURE CAPTIONS

Figure 1 DLTS spectra of (a) the 750°C, and (b) the 900°C annealed O-implanted melt grown ZnO samples. The spectra were taken with $V_R=-1$ V, $V_p=0$ V, and $t_p=1$ ms. The rate window $(\Delta t)^{-1}$ of the measurements varied systemically over a wide range from $\Delta t=0.086$ ms up to 430 ms.

Figure 2 (a) Arrhenius plots of the all the peaks found in the as-O-implanted, 750°C annealed and 900°C annealed ZnO samples. The straight lines are obtained from the fitting assuming a single straight line and the corresponding E_a were shown in the figure; (b) The zoomed-in of the same Arrhenius plots in the high temperature range so that the single peaks data of the as-O-implanted and 750°C annealed sample, as well as those of Peak 3 of the 900°C annealed sample were shown in a larger scale. Single straight line fitting to the data was found in the as-O-implanted sample (see dotted line). However for the 750°C and 900°C sample annealed sample data, significant deviation from single line fitting was observed (see dotted lines). The solid lines are the fitted lines assuming two temperature regions in the fitting process with details described in the text.

Figure 3 Activation energy E_a as a function of the annealing temperature T of the identified single peak in the O-implanted and the 4-folded N-implanted samples assuming the single component peak. The drop of E_a with increasing annealing temperature $\leq 750^\circ\text{C}$ was the effect of the merging of an annealing induced peak

(0.16eV) with the original peak with $E_a \sim -0.29\text{eV}$. New peaks were induced in the 900°C annealed sample spectra. The 0.37 eV peak consisted of the 0.29 eV and 0.58 eV, and the other two peaks had single component.

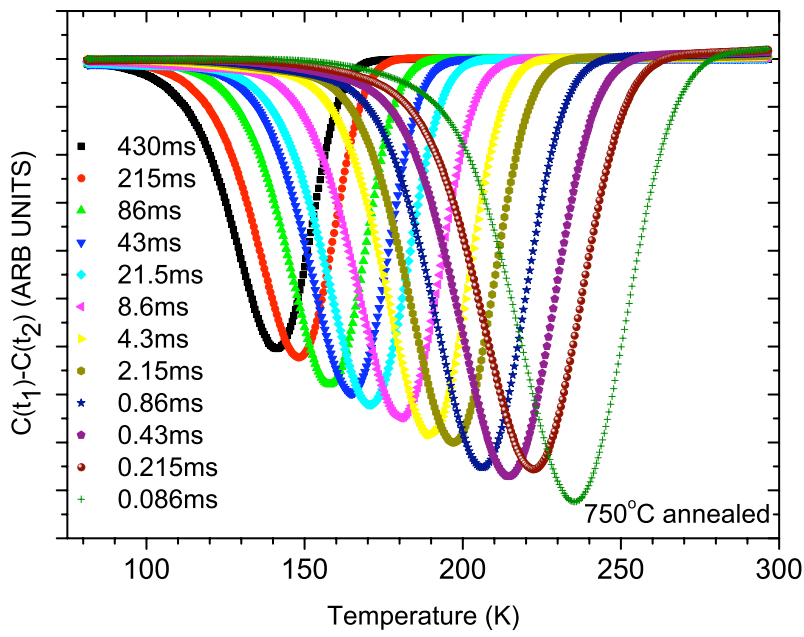


Figure1(a)

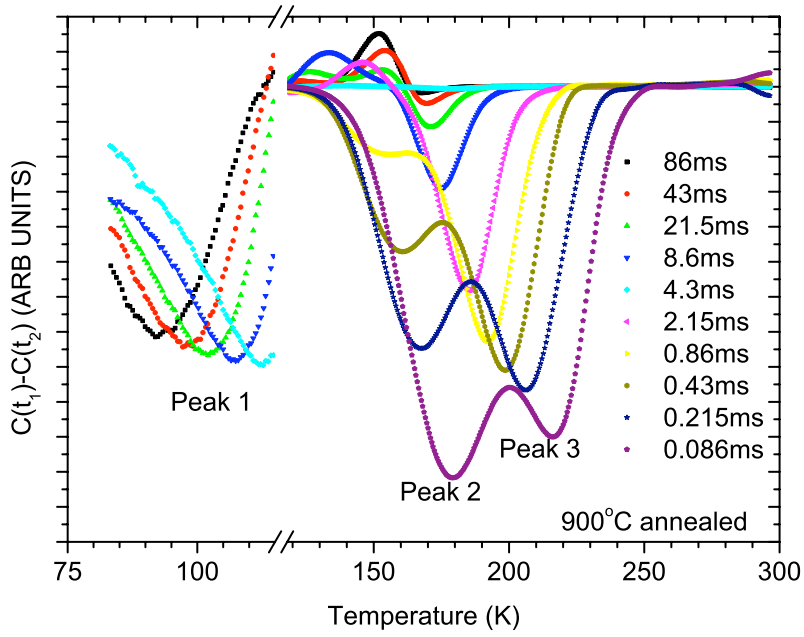


Figure 1(b)

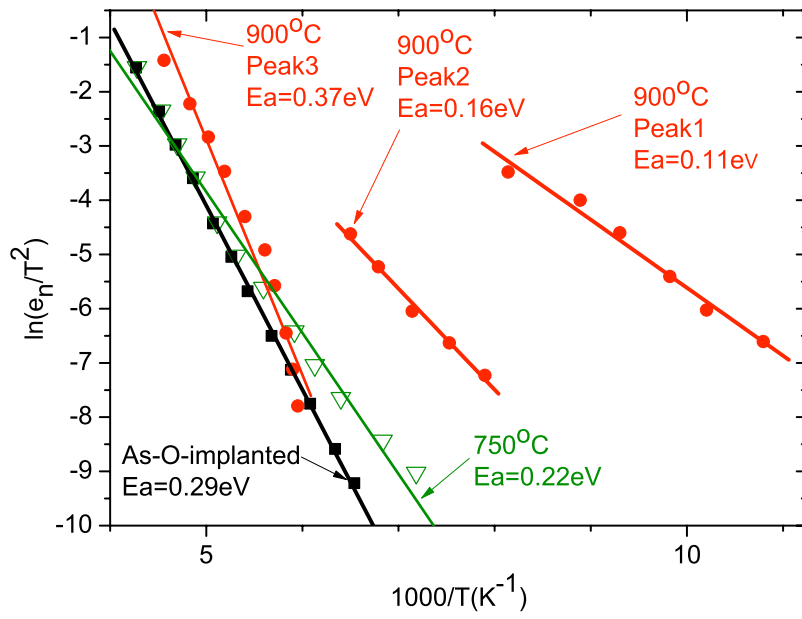


Figure 2(a)

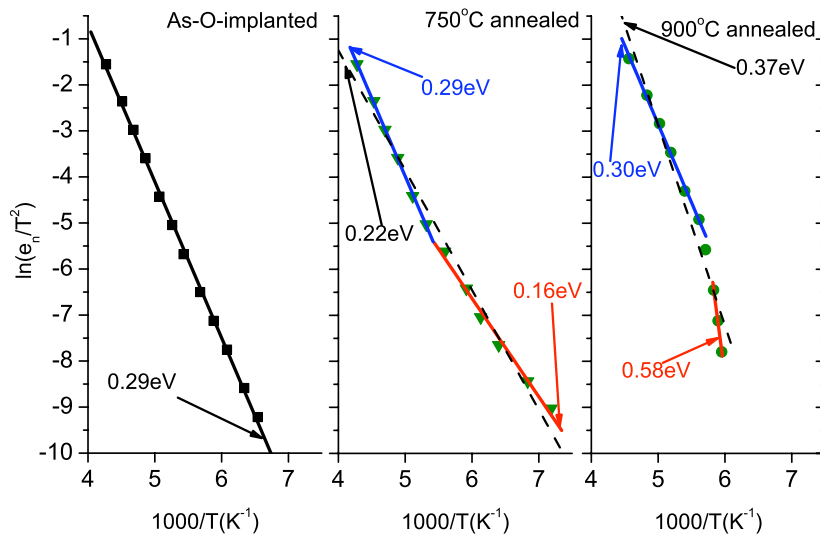


Figure 2(b)

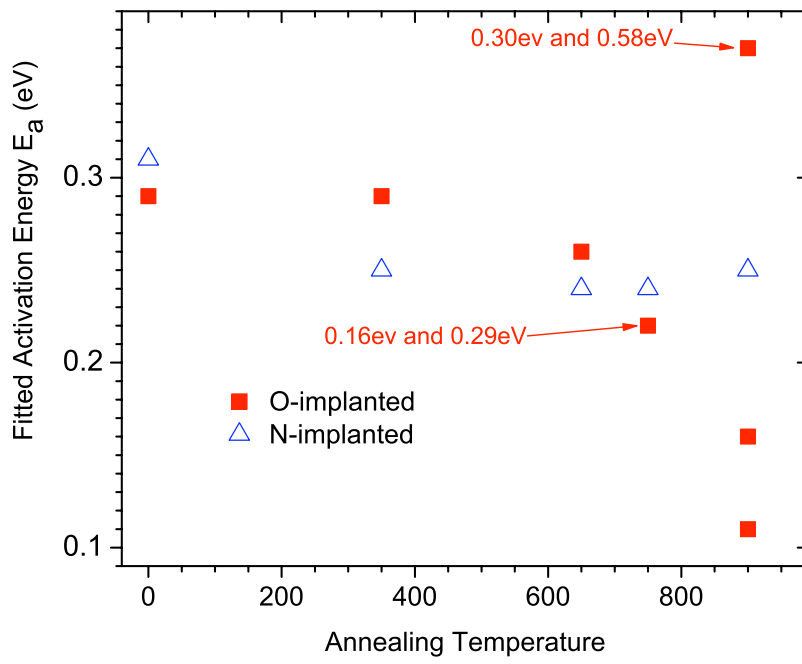


Figure 3